Monitoring of thoracic activity using electromagnetic coupling

Daniel Teichmann, Andreas Kuhn, Dennis De Matteis, Thorsten Bartelt, Marian Walter and Steffen Leonhardt
Philips Chair for Medical Information Technology
RWTH University
Aachen, Germany
Email: teichmann@hia.rwth-aachen.de

***Abstract*—This paper gives an analysis of noncontact monitoring of thoracic activity by electromagnetic coupling between a sensor coil and thoracic tissue (sometimes called Magnetic induction monitoring). In this context, thoracic activity comprises respiratory and cardiac activity as well as further body motion. The physical principle of the measurement technique is described and several wearable and stationary monitoring devices developed by the authors are presented. Sensor characteristics are investigated in laboratory experiments and the suitability of the measurement method for homemonitoring systems is evaluated in different medical applications on healthy volunteers. This work intends to give an overview about the findings achieved by the authors and, therefore, summarizes information already been published elsewhere.**

I. Introduction

The aim of medical homemonitoring systems is to perform a regular and self-actuating monitoring of the health status of elderly and diseased persons, while allowing those persons to stay in their domestic environment. Next to a decrease of the costs for health organizations this would mean a great increase in quality of life for the patients.

A practicable realisation of homemonitoring systems requires special sensor solutions for vital sign monitoring. Suitable sensors should be easy-to-use and easy-to-apply, without the need for precise positioning. Skin irritations by electrodes should be avoided, in order to conduct long-term-measurements. An essential point is the psychological acceptance of the sensors by the patients. For this purpose, the measurement should take place as unobtrusive as possible and the sensors should be integrated into items of daily use, like beds, seats, or clothes.

In this paper, the principle of electromagnetic coupling is analyzed and evaluated for its suitability for unobtrusive monitoring of thoracic activity. Several noncontact or wearable measurement systems developed by the authors are presented. Thoracic activity describes respiratory and cardiac activity as well as further body movement of the thorax.

Since the investigated monitoring technique works in a noncontact way, it fulfills all of the listed requirements of an ideal sensor for medical homemonitoring systems. It is based on electromagnetic coupling between a sensor coil and thoracic tissue and is sometimes called Magnetic induction (MI) monitoring. There are other techniques for magnetic eddy current induction measurements which are based on a multiple coil method [1], [2], [3], [4], [5] using one coil for field excitation and further ones for field measurement. Those multiple coil setups are not considered in this paper, since these methods are not based on coupling in the narrower physical sense of mutual interaction between coil and body.

II. Description of the measurement principle

A. Brief history [6]

The use of magnetic induction measurements for physiological activity monitoring was introduced in 1967 by Vas et al. and called 'Displacement cardiograph' [7] (Wilson et al. later claimed this device to work solely via capacitive coupling [8]). Over the last three decades, the method has occasionally been investigated by four research groups [9], [10], [11], [12]. In addition, a non-wearable system for bedside respiratory monitoring was presented that was also based on a flexible coil [13]. In 2014, a mobile, textile-integrated magnetic induction device was presented by our group [14].

B. Physical Principle [6], [15]

Magnetic induction monitoring is a noncontact technique to assess thoracic activity by measuring the impedance distribution within the thorax.

A sensor coil is driven by an alternating current, so that it excites an alternating magnetic field, $\boldsymbol{B_1}$. $\boldsymbol{B_1}$ induces eddy currents within the thorax. These eddy currents, in turn, excite another alternating magnetic field, $\boldsymbol{B_2}$, whose size and orientation depends on the thoracic impedance distribution. By combining the Biot–Savart law and the law of induction, the elementary component, $\boldsymbol{B_2}$, of the reinduced field caused by the elementary eddy current loop within the field of eddy currents can be calculated by:

$$\boldsymbol{B_2} = -\frac{\mu}{4\pi}\frac{1}{Z_{thorax}}\frac{d\Phi_1}{dt}\int\limits_{\partial S_2} d\boldsymbol{l_2} \times \frac{\boldsymbol{r_2}}{|\boldsymbol{r_2}|^3} \tag{1}$$

where μ denotes the magnetic permeability, Φ_1 denotes the magnetic flux, ∂S_2 describes the boundary curve corresponding to the area, S_2, spanned by the elementary eddy current path, Z_{thorax} denotes the thoracic impedance along the eddy current path, $d\boldsymbol{l_2}$ denotes the infinitesimal length of the current path tangential to the curve, ∂S_2, and $\boldsymbol{r_2}$ is the displacement vector between $d\boldsymbol{l_2}$ and a point in the environment.

According to Lenz's law the change of the secondary magnetic field $d\Phi_2/dt$ is opposed to the change of the primary

one $d\Phi_1/dt$. The secondary magnetic field reinduces a voltage into the coil

$$U_{1,ind} = \frac{\mu}{4\pi} \int_{S_1} \int_{S_2} \int_{\partial S_2} \frac{1}{Z_{thorax}} \frac{d^2 \boldsymbol{B}_1}{dt^2} d\boldsymbol{l_2} \times \frac{\boldsymbol{r_2}}{|\boldsymbol{r_2}|^3} d\boldsymbol{S_2} d\boldsymbol{S_1}, \quad (2)$$

Hence, the coil's impedance takes a new value, the so called reflective impedance $Z_{1,r} = Z_{coil,,r}$.

C. Paths of coupling [15], [16]

The measurement of thoracic activity by electromagnetic coupling can be divided into an inductive and a capacitive coupling path.

The inductive coupling path can be described by a traditional transformer model [17], [18], whose electrical equivalent circuit is shown in Fig. 1. The coil forms the primary

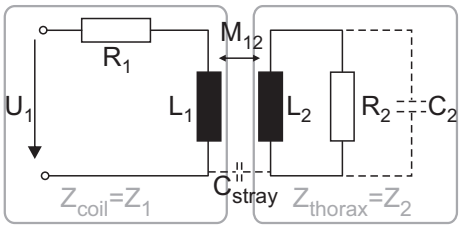

Fig. 1. Electrical equivalent circuit of magnetic induction principle as a transformer model [6].

inductance L_1 and the eddy currents in their collective the secondary one L_2. Resistance R_1 is the series resistance of the coil, while R_2 describes the eddy current losses within the conductive thorax. Dielectric properties of the tissue are abstracted by the capacitance C_2.

Both sides are electromagnetically coupled with each other via the mutual inductance $M_{12} = M_{21}$. It could be shown that the effect of C_2 can be neglected when typical values of human tissues are assumed [16]. Under this assumption the primary reflective impedance due to inductive coupling splitted into its real and imaginary part can be calculated by:

$$Re\{Z_{l,r}\} = \underbrace{R_1}_{R_{l,0}} + \underbrace{\frac{\omega^2 L_1 L_2 k^2 R_2}{\omega^2 L_2^2 + R_2^2}}_{\Delta R_l} \quad (3)$$

$$Im\{Z_{l,r}\} = \omega(\underbrace{L_1}_{L_{l,0}} - \underbrace{\frac{\omega^2 L_1 L_2 k^2 L_2}{\omega^2 L_2^2 + R_2^2}}_{\Delta L_l}), \quad (4)$$

Next to the inductive coupling path, there also exists a capacitive path over the stray capacitance C_{stray} (see Fig. 1) between coil surface and thoracic wall. C_{stray} can have a significant affect on the measured signal when the dstance between coil and thorax varies. Furthermore, there may exist parasitic inductive coupling M_{stray} due to displacement currents over C_{stray}. The reflective primary capacitance $C_{1,r}$ is composed by the originally existing capacitive content of the primary LCR-net C_1 (consisting of stray capacitance between coil windings and further oscillatory capacitors) and the stray capacitance C_{stray} generated by coupling between body and coil:

$$C_{1,r} = \underbrace{C_1}_{C_{1,0}} + \underbrace{C_{stray}}_{\Delta C_1}. \quad (5)$$

C_{stray} can be described by

$$C_{stray} = a_c \frac{1}{d}, \quad (6)$$

where a_c is a constant and d is the distance between coil surface and thoracic wall. This means that the primary capacitance $C_{1,r}$ increases with decreasing distance d [18].

D. Paths of modulation

There are three different ways in which thoracic activity can modulate the reflected impedance of the coil enabling vital sign monitoring by electromagnetic coupling. These paths of modulation are described in the following [19], [16].

1) Thoracic impedance (volume change, boundary displacement): The volumes of organs, tissue or blood can be varied by physiological activity. This may change the conductivity within a specific body region and influence the current strength. Furthermore, the displacement of inner and outer boundaries of organs changes the direction of current paths and, hence, the resistivity along the current path. It can be subdivided into three types of impedance modulation [20], [16]:

- Type I: Volume change *(e.g. increase of blood volume in the heart during diastole)*
  The volume of organs, tissue or blood can be varied by physiological activity. This may change the conductivity within a specific body region and influences the current strength.
- Type II: Boundary displacement *(e.g. lifting of the heart during inspiration, closing of the heart valves)*
  The displacement of inner and outer boundaries of organs changes the direction of current paths.
- Type III: Microscopic processes *(e.g. changes in ionic concentration)*
  Microscopic processes may vary electric properties of tissue or blood. This modulation type is of minor influence when monitoring short-periodic vital signs, since physiological microscopic processes should take place very slowly.

2) Distance [19]: A variation in the distance between the sensor and the thoracic wall (or other tissue boundaries) modifies the magnetic coupling factor, k, and has, therewith, direct influence on the reflective coil impedance via inductive coupling. Furthermore, a change in distance the also affects the amount of capacitive stray coupling.

3) Deflection [19]: A change in the form of the coil (by bending) or the eddy current paths (by organ displacement) would change k, as well as the primary (L_{coil}) or secondary (L_{eddy}) self-inductance.

E. Technical Realization

The described principle of magnetic induction measurement is based on an impedance change of a measurement coil evoked by thoracic activity of a body, which is electromagnetically coupled with the coil. The measurement systems presented in Section II-F are using either a Frequency (FM) or Amplitude modulation (AM) approach for obtaining changes of the coil's impedance while simultaneously sending out the excitation field. In both methods the coil is the inductive part of a LCR-tank.

When using the FM method, the coil is a frequency determining part of an oscillator. Hence, if the impedance of the coil changes due to thoracic activity, the oscillatory frequency changes as well. This frequency change can be recorded by means of a frequency counter. For this purpose, the output of the oscillator is rectified and passed to the counter input of a microcontroller [16].

Magnetic induction monitoring via Amplitude demodulation is based on a complex voltage divider consisting of a resistor R_{pre} and the LCR-tank. The voltage divider is driven by an alternating voltage of constant amplitude and frequency. The amplitude and phase of the voltage E_{meas} measured between R_{pre} and the LCR-Tank vary, when the reflected impedance of the coil changes due to thoracic activity. This effect is measured by an amplitude demodulation circuit [21].

F. Measurement Systems

Five different devices for thoracic activity monitoring by electromagnetic coupling according to the technical description in Section II-E have been developed. Two of them are dedicated for mobile use, while the other ones are stationary systems, which are exemplary integrated or attached to the backrest of a chair.

1) Stationary Measurement Systems:

a) Stationary system based on FM read-out technique (FM system): The measurement is etched on a rigid printed circuit board. It consists of one winding and a diameter of 9 cm. The oscillatory frequency is 14 MHz. As it can be seen in Fig. 2(a) the measurement system is attached on the backrest of chair.

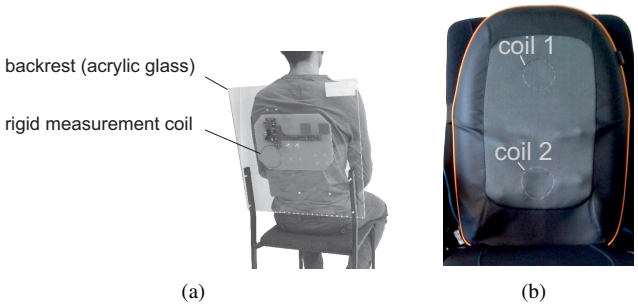

Fig. 2. Photographs of stationary measurement systems on basis of the FM read-out technique with (a) rigid (FM system) and (b) flexible (FM_{flex} system) measurement coils. [22], [23].

b) Stationary system based on FM read-out technique using bendable coils (FM_{flex} system): The FM_{flex} system (see Fig. 2(b)) comprises two measurement channels, which are based on the same technique as the system described in the preceding Section. The differences is that the coils are bendable. This was achieved by using high frequency litz wire, which has been sewn into the seat cover. The measurement coils have a diameter of 75 mm and three winding. The oscillatory frequencies are both adjusted to 19 MHz.

c) Stationary system based on AM read-out technique (AM system): The AM system comprises three magnetic induction sensors based on the amplitude modulation technique. The coils consist of one winding and have a diameter of 90 mm. The coils' inductivity is 0.36 µH. The resonance frequency of the LCR-nets without a body in their vicinity are adjusted to $f_{res,1} = 10\,\text{MHz}$, $f_{res,2} = 14\,\text{MHz}$, and $f_{res,3} = 19\,\text{MHz}$.

2) Wearable measurement systems:

a) Textile integrated system (MAIN-Shirt): For unobtrusive integration into wearable textiles the measurement system has to be flexible. For this reason the coils are realized by high frequency litz wire sewn into a T-shirt on selected positons. The litz wire has a diameter of 0.2 mm and consists of 460 single strands. In Fig. 3(a) and 3(b) a photograph of the system (called MAIN shirt, for MAgnetic INduction [24]) is given. The system comprises four MI sensors. The impedance modulation is based on the FM technique due to its small amount of required electronic components, so that the complete readout-electronic finds place on a small, onesided flexible printed circuit board (see Fig. 3(c)). The position and the adjusted parameters of each sensor can be found in Table I.

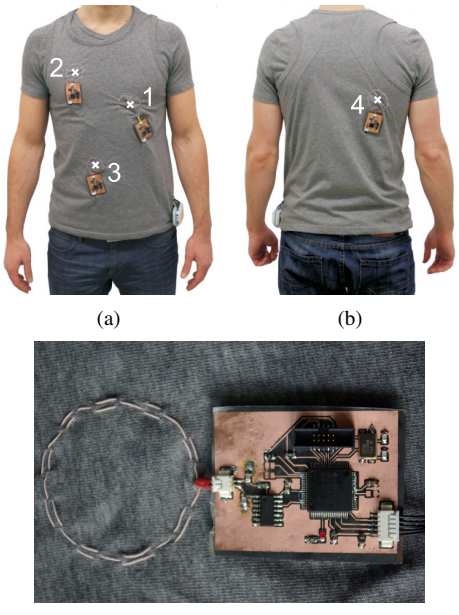

Fig. 3. Textile integrated measurement system (MAIN shirt). Three sensors are positioned on the (a) front and one on the (b) back side of the thorax (centers of the coils are marked); (c) close-up of a single sensor [24].

b) Bendable on-body sensor (FlexPock): Figure 4 shows the system overview of the developed bendable on-

TABLE I. COIL PARAMETERS OF THE MAIN SHIRT WITH RADIUS r, NUMBER OF WINDINGS n, AND BASE FREQUENCY f_0.

Nr.	Position	r [mm]	n	f_0 [MHz]
1	chest, left side, beneath	3,00	3	17
2	chest, right side, above	2,25	3	20
3	abdomen, right	2,25	3	20
4	back, right side	3,00	3	17

body sensor. Due to its pocket-sized flexible construction it is called FlexPock [6]. This measurement system combines a MI sensor with a reflective photoplethysmographic (rPPG) sensor. The data are collected by a microcontroller and transmitted via Bluetooth (BlueMod+B20/BT2.1, Stollmann) to a display unit (PC or android smartphone). The device is powered by a lithium polymer battery, which can be charged by a power-managment circuitry placed beneath the battery. Figure 4(b)

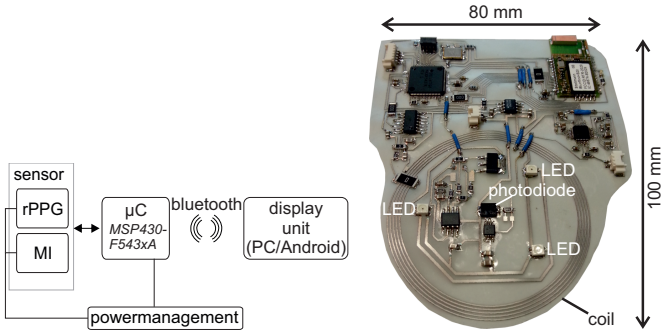

(a) (b)

Fig. 4. Bendable on-body sensor (FlexPock). (a) System overview and (b) photograph [6]

presents a photograph of the actual system. The complete electronic is placed on a bendable printed circuit board, so that the device can adapt to body motion. The coil is etched on the flexible board in form of a pancake coil (outer diameter: 60 mm, number of windings: $n = 5$). The measurement unit of the rPPG sensor is placed in the middle of the coil. Due to its small and flat physical dimension (80 mm x 100 mm x 5 mm) the device fits into a shirt pocket or the inner pocket of a jacket.

III. SENSOR RESPONSE AND MEASURING DEPTH [19]

A. Setup

The sensor coil was placed beneath a cylindrical reservoir filled with saline solution. In the middle of this reservoir is a channel that serves as a check rail for another, smaller tank (sample) filled with saline solution, whose conductivity, σ_{sample}, was varied during the experiment. The diameters of the reservoir and the sample tank were 8.5 and 4.5 cm, respectively. Both were made of polypropylene. The sample tank was weighted with pebble stones and could be lifted by a DC motor. The sample conductivity ranged from $\sigma_{sample} = 1$ ms/cm to $\sigma_{sample} = 8$ ms/cm to represent different organ and tissue types (see Table II) [25], [26], [27]. The conductivity of the saline solution within the cylindrical reservoir acting as the surrounding tissue was $\sigma_{tank} = 1$ ms/cm. This allowed us to compare the change of the sensor signal due to object motion with the change due to object conductivity. The sensor was FM based with a base frequency of 17 MHz, with five windings, and a coil diameter of 60 mm.

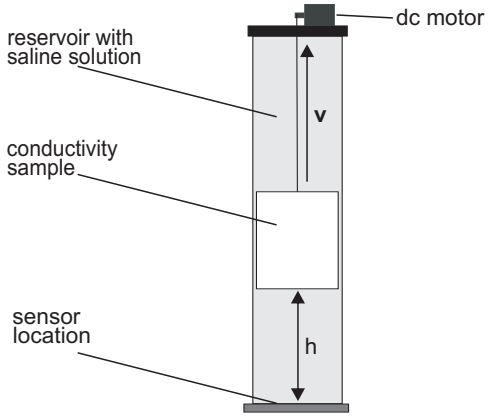

Fig. 5. Measurement setup for the examination of sensor response and measuring depth [19].

TABLE II. SAMPLE CONDUCTIVITY, σ_{sample}, AND THE CORRESPONDING TISSUE TYPES [25], [26], [27] FROM [19].

σ_{sample}	Tissue
1 ms/cm	bone, fat
2 ms/cm	lungs (inspiratory), skin (dry), spinal cord
4 ms/cm	lungs (expiratory), blood vessel, aorta, skin (damp)
6 ms/cm	muscle, heart
8 ms/cm	blood

B. Results

Based on the experimental setup described in the preceding Section, Figure III-B presents the signal output, Δf, of the sensor caused by conductive samples in relation to the sensor-to-object distance, h. The small oscillations in the decreasing tails are presumably caused by the swinging of the sample tank or by a non-smooth characteristic of the DC motor and its cable winch.

To evaluate the impact of organ displacement and organ conductivity on the sensor signal during a cardiac cycle, we examine the sensor's sensitivity at h = 3.5 cm for σ_{sample} = 6 ms/cm and f_0 = 17 MHz in more detail. This point is chosen based on magnetic resonance imaging (MRI) data from one of our monitored volunteers [28]. Using these MRI data, the distance between the heart wall and a sensor coil placed at position 1 (see Figure 3(a)) was determined to range approximately from three to 4 cm during a cardiac cycle. Furthermore, according to Table II, the average conductivity of the heart during diastole and systole is assumed to change 6–8 ms/cm, respectively. Linearization at this point (as shown in Figure III-B, dashed line) yields a sensitivity on object motion of S_{motion} = 86 Hz/cm, while the sensitivity on object conductivity at this distance is S_{cond} = 28 Hz/(2ms/cm) = 14 Hz/(ms/cm). Given that these assumptions are valid, this would mean that during a heart beat, the impact of heart displacement on the sensor signal should be 3.1 times higher than that of heart conductivity changes.

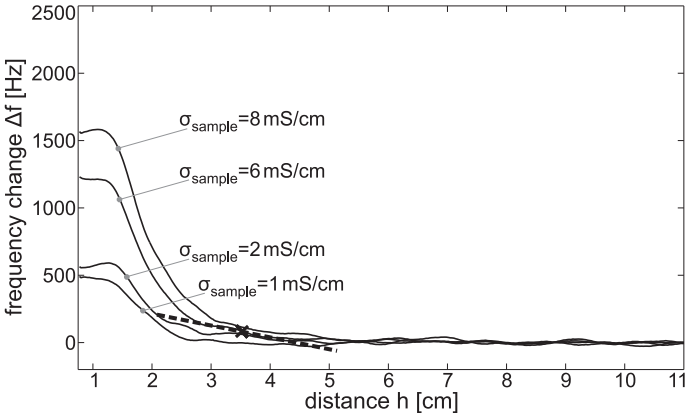

Fig. 6. Results of the examination of sensor response and measuring depth. The signal output, Δf, is presented in relation to the signal-to-object distance (height h), with σ_{sample} being the conductivity of the sample object. Base frequency f_0 is 17 MHz, coil diameter is 60 mm, and number of winding n is 5. [19]

IV. Medical Application of the Measurement Principle

In this section, the technique of thoracic activity monitoring by electromagnetic coupling is tested in different medical applications. In Section IV-A, the signal quality for pulse and respiration monitoring of all measurement systems described in Section II-F are compared and an algorithm for real-time extraction of pulse and respiratory rate is proposed.

In Section IV-B the feasibility of non-invasive continuous cardiac output estimation by electromagnetic coupling is investigated.

For proper evaluation of a patients health and well-being, besides assessment of vital signs, monitoring of the patients activity is an additional essential requirement. This includes quantification of the activity level as well as the generation of emergency alerts, e.g. fall detection. Therefore, recognition of motion patterns for instant classification of personal physical activities should be a basic feature in telemonitoring healthcare [30]. Therefore, in Section IV-C the applicability of magnetic induction measurement for motion classification is analyzed.

A. Monitoring of pulse and respiratory rate

1) Comparison of signal quality [22]: Two volunteers have been asked to conduct a measurement with all measurement systems presented in Section II-F while performing the following measurement protocol: 30 sec normal breathing, 15 sec apnea, 30 sec normal breathing. For the FM system a PPG sensor (ChipOx, Corscience) and a flow meter (Model 4040, TSI) was used as cardiac and respiratory reference. In case of the other systems, a patient monitor (IntelliVue MP 70, Philips), more specific the ecg and bioimpedance signal, was used for cardiac and respiratory reference, respectively. The measurement position of the stationary systems was on the left thorax back side at the height of the heart. For the MAIN shirt, position 1 (front, above the heart) was used for the comparison.

In order to compare the signal quality, the following criteria are introduced.

- *peak-to-peak output (p-p$_{cycle}$)*: average peak-to-peak amplitude (output) of the signal during a respiratory or cardiac cycle. For FM based sensors the signal output is the change in frequency Δf, for the AM based device it is the measured voltage over the LCR-net $\Delta|U_{meas}|$.
- *Signal-to-noise ratio (SNR)*: ratio in decibel (dB) between p-p$_{cycle}$ and the noise floor (two times the root mean square). Noise was defined as all signal content above the corner frequency of 20 Hz.

Figure 7 shows exemplary the sensor signal during the complete measurement period for the FM system and a close up on two respiratory cycles and 10 sec of apnea for the FM$_{Flex}$ and FlexPock device.

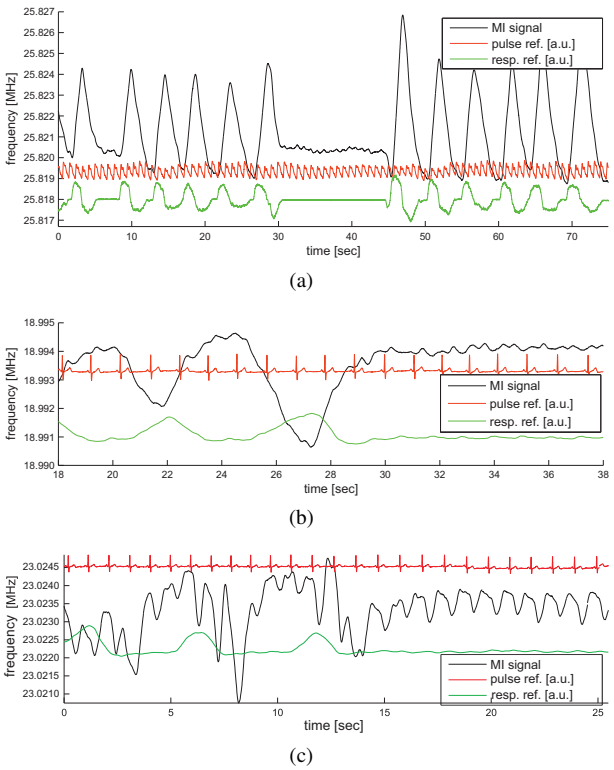

Fig. 7. Exemplary signal excerpts obtained in measurements with an healthy volunteer using the (a) FM , (b) FM $_{flex}$, and (c) FlexPock system. (a) shows the whole measurement period (30 sec normal breathign, 15 sec apnea, 30 sec normal breathing), (b) and (c) show a close-up onto 2 respiratory cycles and 10 sec of apnea [22].

Table III lists the SNR for the respiratory and cardiac (during apnea) signal. A comparison of the ratio between p-p$_{resp}$ and p-p$_{pulse}$ is also given.

All stationary systems provide good respiratory information with high SNR values between 60.8 dB and 127.0 dB. The cardiac signal shows a much lower signal amplitude and is overlayed by the respiratory signal. Apparently, the AM signal has lower SNR, but also a lower ratio between respiration and pulse of only 3.5, which would simplify pulse detection.

The cardiac signal content of the wearable measurement systems (MAIN shirt and FlexPock device) is significantly higher. This is caused by the sensor position on the front,

which is nearer to the heart than for the stationary systems, and by the flexible coil realization, which allows a further modulation of the signal by bending (see Section II-D).

TABLE III. CALCULATED QUALITY CRITERIA. VALUES ARE AVERAGED OVER ALL VOLUNTEERS.

	measurement system				
criterion	FM	FM_{Flex}	AM_{AM}	MAIN shirt	FlexPock
SNR_{resp} [dB]	127.0	107.3	60.8	107.0	100.9
SNR_{pulse} [dB]	47.2	53.2	39.0	61.7	75.6
$p\text{-}p_{resp}/p\text{-}p_{pulse}$	54.1	16.1	3.5	6.2	3.6

2) Algorithm for the extraction of pulse and respiration rate during breathing and slight walking: For the use of electromagnetic coupling for unobtrusive measurements in homemonitoring systems, an automatic extraction of pulse and respiration rate is necessary. The signal processing should take place in real-time, so that a critical health status can be detected immediately. Mobility and motion of the monitored person should not restricted. Therefore, motion artefacts will be produced, which have to detected. A further challenge for an automatic extraction algorithm is the fact that the cardiac signal is overlayed by a significantly higher respiratory signal content.

In Fig. 8 a flow chart of the proposed algorithm is presented. By subdividing the raw signal into several subbands

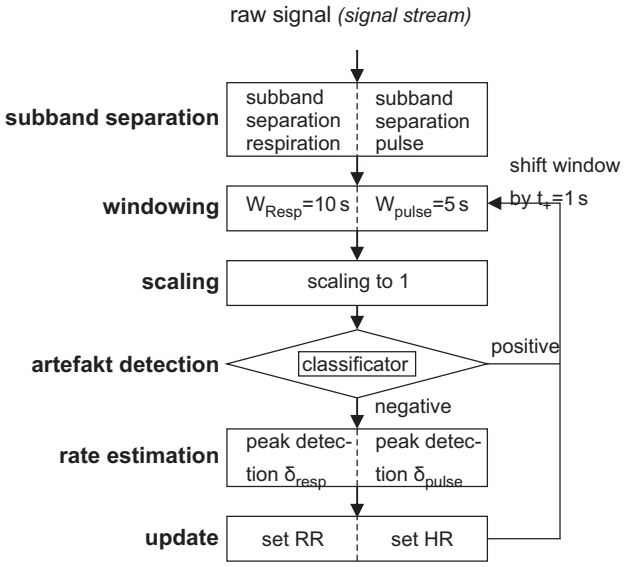

Fig. 8. Flow chart of the proposed algorithm for pulse and respiration rate extraction. modified from [22]

by discrete wavelet transform (DWT), the respiratory and cardiac signals are separated from each other. Following, the selected subbands are windowed. To ensure a correct parameter extraction each window is checked for artefacts by a k-nearest-neighbour classificator (using DWT based features) and is only used for the estimation of the period length, if it does not include any artefacts.

The described algorithm was applied to signals recorded with the MAIN shirt. For this purpose, measurements of 150 sec of normal breathing were recorded on eight volunteers during standing posture, sitting posture and slow walking. Additionally, 20 sec of apnea were recorded in standing posture. For each measurement, the sensor position with the highest heart-signal-coverage was chosen for further processing.

The algorithm was applied to the data using coiflet5 wavelets, a window length of 10 sec, and a moving average over five calculated beat-to-beat intervals. Table IV gives the

TABLE IV. VALUE OF THE AVERAGE RELATIVE ERROR, $\bar{F}_{rel,pulse}$, OF THE CALCULATED BEAT-TO-BEAT INTERVALS $BB_{MI,10}$ DURING DIFFERENT POSTURES AND ACTIVITIES. [22]

posture/activity	$\bar{F}_{rel,pulse}$ [%]
Standing	5,0
Sitting	5,8
Walking	4,2
Apnea	5,5
Mean	*5,1*

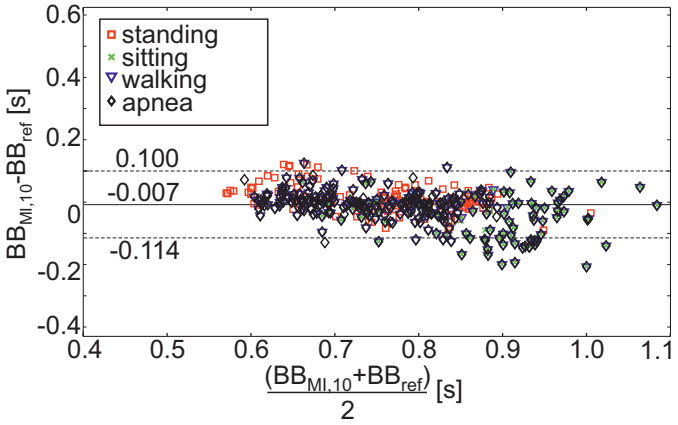

Fig. 9. Bland-Altman plot: Comparison of the Beat-to-Beat intervals extracted from the MAIN shirt signal $BB_{MI,10}$ with the beat-to-beat intervals of the reference system BB_{ref} during different postures and activities [19].

average relative errors $\bar{F}_{rel,pulse}$ of the extracted beat-to-beat intervals $BB_{MI,10}$ for each posture and activity compared to the reference BB_{ref} (PPG, ChipOx, Corscience). Furthermore, Fig. 9 illustrates the result in a Bland-Altman plot.

B. Cardiac Output estimation

Aim of this experiment, was to conduct a proof of concept that a non-invasive and continuous estimation of cardiac output (CO) by means of electromagnetic coupling is feasible. Data were acquired with the MAIN shirt (position 1) on one healthy volunteer. The reference device was an Impedance cardiography device (Niccomo, medis GmbH, Germany). Its estimation of the CO is based on changes of the thoracic impedance distribution evoked by the blood volume that is ejected by the heart into the aorta. The ICG device uses four electrodes, whose positions are shown in Fig. 10.

The volunteer performed the following measurement protocol. After a baseline phase, he performed three activity phases (five minutes) each followed by a six minute measurement phase in sitting posture. During this measurement phase the volunteer held his breath for 20 sec every 40 sec. Solely the signal periods recorded during these apnea phases were used for CO estimation.

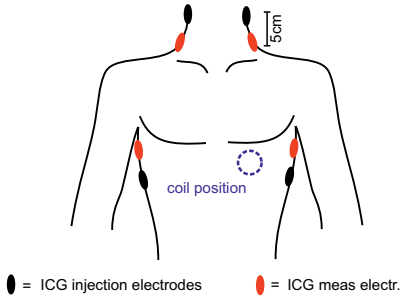

Fig. 10. Position of the measurement coil of the MI sensor and the electrodes of the ICG reference [22].

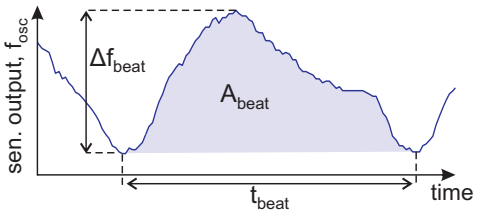

Fig. 11. Typical signal of the MI device during one heart beat and the parameters extracted for cardiac output estimation [14].

After highpass filtering of the MI signal with a corner frequency of 0.5 Hz, each single heart beat recorded during the apnea phases was segmented and its length t_{beat}, area under the curve A_{beat}, and maximum signal amplitude (i.e. frequency shift) Δf_{beat} was extracted. Due to the high standard deviation between beat-to-beat recorded CO values, it is recommended by the manufacturer of the reference device to average the results over several beats. Thus, a moving average of 8 beats was applied to the reference as well as to the MI signal. [14]

The correlation between the extracted heartbeat parameters and the corresponding stroke volume recorded by the reference device (SV_{ref}) was determined by regression analysis. The regression model was based on the two-element windkessel model. The windkessel model describes the relation between arterial blood pressure and volume flow by fluid dynamics and is the basic theoretical model for pulse contour analysis [31]. Substituting pulse contour by the MI signal yielded to the following regression model (heart rate (HR) was additionally added):

$$\mathrm{SV} = \alpha \cdot A_{beat} + \beta \cdot \Delta f_{beat} + \gamma \cdot \mathrm{HR} + \delta \tag{7}$$

Afterwards, the cardiac output was calculated out of the stroke volume (SV) by:

$$\mathrm{CO} = \mathrm{SV} \cdot \frac{1}{t_{beat}}. \tag{8}$$

The result of this analysis is shown in Fig. 12 by means of a Bland-Altman plot. The CO estimation has been performed separately for each measurement phase. The mean deviation of the calculated CO is -0.03 l/min, the standard deviation is about 0.35 l/min. There are no apparent systematic trends at regions with higher or lower CO values. High deviations seem to tend towards lower values. The percentage error (PE) is 12.68 % and, therewith, within the region of clinical relevance [32].

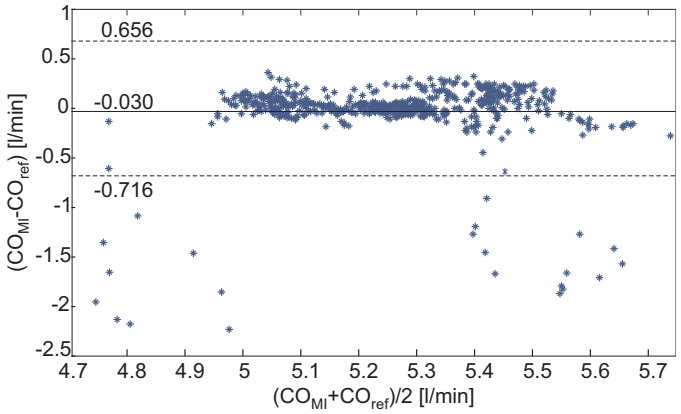

Fig. 12. Bland-Altman Plot of the estimated cardiac output values (CO_{MI}) in comparison to the reference system (CO_{ref}) [22].

C. Motion Classification [30]

A great difficulty in measurements of cardiorespiratory activity by electromagnetic coupling is the strong sensitivity to motion, yielding to a high number of motion artefacts. However, those occuring motion artefacts include a lot of useful information about the movements performed by the monitored person and can be used for the classification of motion patterns.

To proof this concept nine healthy volunteers performed the following motion patterns for 150 sec while wearing the MAIN shirt:

- Standing
- Sitting
- Slow walking (0.9 mph)
- Fast walking (2.8 mph)
- Jogging (2.8 mph)

'Jogging' was performed with the same speed of 2.8 mph as 'Fast walking', to ensure that the distinction between both patterns is based on the trajectory rather than on speed.

The recorded time periods were divided into segments of 30 s, 15 s, 10 s and 5 s, in order to investigate the time length required of a sample for a good classification result. Therefore, depending on the time period being investigated, 45, 90, 135 or 270 samples per class of motion pattern were available. From this data pool, a training data set was generated separately for each sample being tested by using all the remaining data as the training data set (randomized cross validation [33]). [30]

Three different classification algorithms were tested for their suitability. Those were Bootstrap aggregating decision trees (BDT), Artificial neural networks (ANN), and Support vector machines (SVM). The calculated features used for the classifications are given in Table V. Figure 13 shows the misclassification error (MRE) for all classificators in dependence on the sample length. The BDT classificator produces the lowest error. With a sample length of 30 sec it produces a MRE of 0.4, i.e. only 4% of the test data was misclassified. Figure 14 compares the performance of the different classification algorithms by means of sensitivity and specificity (each

TABLE V. CALCULATED FEATURES FOR CLASSIFICATION OF MOTION PATTERNS [30].

Domain	Feature	
time-frequ.	x_1: total energy of all DWT levels E_T	
	x_2: relative energy of DWT approximation $\frac{E_A}{E_T}$	
	x_{3-8}: relative energy in single DWT levels $\frac{E_{D,1-6}}{E_T}$	
time	x_9: average,	$\mu = \frac{1}{n}\sum_{i=1}^{n} s_i$
	x_{10}: standard deviation,	$\sigma = \sqrt{\frac{1}{n-1}\sum_{i=1}^{n}(s_i-\mu)^2}$
	x_{11}: skewness,	$v = \frac{1}{n}\sum_{i=1}^{n}(\frac{s_i-\mu}{\sigma})^3$
	x_{12}: kurtosis,	$w = \frac{1}{n}\sum_{i=1}^{n}(\frac{s_i-\mu}{\sigma})^4$
	x_{13}: peak-to-peak value,	$p = \max(\mathbf{s}) - \min(\mathbf{s})$

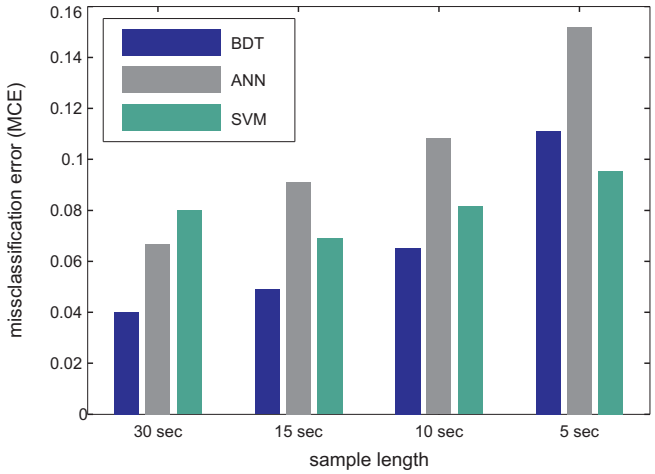

Fig. 13. Misclassification error of all the classifiers for different sample lengths [30].

for its best sample length). The performance of ANN and SVM are in a similiar range, while the BDT provides the best result for both quality criteria.

V. DISCUSSION AND CONCLUSION

The laboratory experiment confirmed the assumed physical principle. Sensors based on the electromagnetic coupling between the thorax and a measurement coil measure the conductivity distribution within an object and are sensitive to the displacement and the changes in the conductivity of organs. The impact of heart motion on the signal is estimated to be 3.1 times higher than the impact of heart conductivity changes during a cardiac cycle.

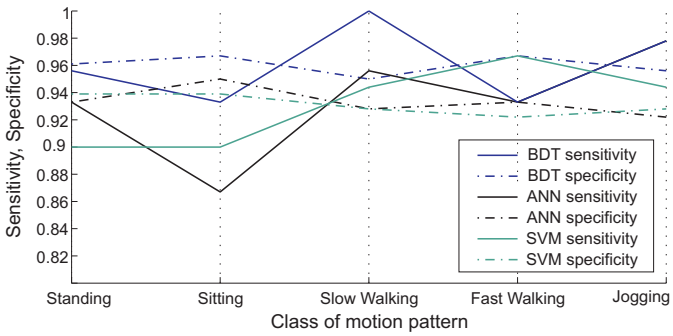

Fig. 14. Sensitivity and specificity for each class and each classifier [30].

Noninvasive estimation of cardiac output using electromagnetic coupling achieved good results. However, a drawback is that due to changes in form and position of the measurement coil a calibration had to be performed after each motion phase. This problem could be eliminated by a tighter attachement of the coil.

The use of the sensors' sensitivity to motion for motion pattern classification is a new application area and seems to have promising potential. The experiments indicate the feasibility of magnetic induction sensors for the detection and classification of motion patterns. With the presented magnetic induction device, all tested classifiers were able to classify the defined motion pattern with an accuracy of over 93 %. Overall, the proposed decision tree algorithm produces the best classification performance (accuracy of 96 %), while the SVM seems the most suitable for realtime application. As a next step the feature space should be reduced.

In view of the sensors' ability to monitor cardiac and respiratory activity as well as further motion-related activity, and their seamless integration into items of daily-use, electromagnetic coupling based monitoring seems to be a convenient method for home monitoring applications.

REFERENCES

[1] P. P. Tarjan and R. McFee, "Electrodeless measurements of the effective resistivity of the human torso and head by magnetic induction," *IEEE Transactions on Biomedical Engineering*, vol. 15, no. 4, pp. 266–278, 1968.

[2] H. Griffiths, "Magnetic induction tomography," *Measurement Science and Technology*, vol. 12, no. 8, pp. 1126–1131, 2001.

[3] H. Scharfetter, H. K. Lackner, and J. Rosell, "Magnetic induction tomography: hardware for multi-frequency measurements in biological tissues," *Physiological measurement*, vol. 22, no. 1, pp. 131–146, 2001.

[4] C. H. Riedel, "Planar inductive impedance measurement methods in medical engineering (germ.)," Ph.D. dissertation, Fridericiana Karlsruhe University, Karlsruhe, 2004.

[5] A. Cordes, J. Foussier, D. Pollig, and S. Leonhardt, "A portable magnetic induction measurement system (PIMS)," *Biomedizinische Technik/Biomedical Engineering*, vol. 57, no. 2, pp. 131–138, 2012.

[6] D. Teichmann, D. D. Matteis, T. Bartelt, M. Walter, and S. Leonhardt, "A Bendable and Wearable Cardiorespiratory Monitoring Device Fusing Two Noncontact Sensor Principles," *IEEE journal of biomedical and health informatics*, 2015.

[7] R. Vas, "Electronic device for physiological kinetic measurements and detection of extraneous bodies," *IEEE Transactions on Biomedical Engineering*, vol. BME-14, no. 1, pp. 2–6, 1967.

[8] D. L. Wilson and D. B. Geselowitz, "Physical principles of the displacement cardiograph including a new device sensitive to variations in torso resistivity," *IEEE Transactions on Biomedical Engineering*, vol. BME-28, no. 10, pp. 702–710, 1981.

[9] M. C. Kwok and M. G. Pepper, "Noninvasive detection of ventricular wall motion by electromagnetic coupling: Part 1 Theory," *Medical & Biological Engineering & Computing*, vol. 29, no. 2, pp. 136–140, 1991.

[10] R. Guardo, S. Trudelle, A. Adler, C. Boulay, and P. Savard, "Contactless recording of cardiac related thoracic conductivity changes," in *Annual International Conference of the IEEE Engineering in Medicine and Biology Society (EMBC)*, vol. 2, Quebec, Canada, 20-24 Sep 1995, pp. 1581–1582.

[11] L.-H. Humal and J. Vedru, "Physiological measurement based on foucault principle: set-up of the problem," in *1st International Conference on Bioelectromagnetism*, Tampere, Finland, 9-13 June 1996.

[12] M. Steffen, A. Aleksandrowicz, and S. Leonhardt, "Mobile noncontact monitoring of heart and lung activity," *IEEE Transactions on Biomedical Circuits and Systems*, vol. 1, no. 4, pp. 250–257, 2007.

[13] A. Richer and A. Adler, "Eddy current based flexible sensor for contactless measurement of breathing," in *IEEE Instrumentation and Measurement Technology Conference (IMTC)*, Ottawa, Canada, 16-19 May 2005, pp. 257–260.

[14] D. Teichmann, T. Bartelt, S. Leonhardt, and M. Walter, "A mobile and wireless approach for cardiac output monitoring," in *IEEE Topical Conference on Biomedical Wireless Technologies, Networks & Sensing Systems (BioWireleSS)*, 19-22 Jan 2014.

[15] Daniel Teichmann, *Kontaktlose Erfassung thorakaler Aktivität mittels elektromagnetischer kopplung: Dissertation - phd thesis*. Germany: Shaker Verlag, 2015.

[16] D. Teichmann, J. Foussier, J. Jia, S. Leonhardt, and M. Walter, "Noncontact monitoring of cardiorespiratory activity by electromagnetic coupling," *IEEE Transactions on Biomedical Engineering*, vol. 60, no. 8, pp. 2142–2152, 2013.

[17] H. L. Libby, *Introduction to Electromagnetic Nondestructive Test Methods*. Huntington: R. E. Krieger Pub. Co., 1979, c1971.

[18] M. G. Pepper, D. J. E. Taylor, and M. C. Kwok, "Noninvasive detection of ventricular wall motion by electromagnetic coupling: Part 2: Experimental," *Medical & Biological Engineering & Computing*, vol. 29, no. 2, pp. 141–148, 1991.

[19] D. Teichmann, A. Kuhn, S. Leonhardt, and M. Walter, "The MAIN Shirt: A textile-integrated magnetic induction sensor array," *Sensors (Basel, Switzerland)*, vol. 14, no. 1, pp. 1039–1056, 2014.

[20] M. Steffen, "Non-contact monitoring of heart and respiratory activity using magnetic induction (germ.)," Ph.D. dissertation, RWTH Aachen University, Aachen, 2009.

[21] D. Teichmann, J. Foussier, and S. Leonhardt, "Respiration monitoring based on magnetic induction using a single coil," in *IEEE Biomedical Circuits and Systems Conference (BioCAS)*, Paphos, Cyprus, 3-5 Nov 2010, pp. 37–40.

[22] Daniel Teichmann, "Kontaktlose erfassung thorakaler Aktivität mittels elektromagnetischer kopplung," Ph.D. dissertation, RWTH Aachen University, 2015.

[23] D. Teichmann, J. Foussier, J. Jia, and S. Leonhardt, "Non-contacting monitoring of respiration and pulse based on capacitive coupling with thoracic tissue," in *World Congress on Engineering (WCE)*, vol. 3, London, UK, 6-8 July 2011.

[24] D. Teichmann, D. D. Matteis, M. Walter, and S. Leonhardt, "A bendable and wearable cardiorespiratory monitoring device fusing two noncontact sensor principles," in *11th International Conference on Wearable and Implantable Body Sensor Networks (BSN)*, Zurich, Switzerland, June 16-20 2014, pp. 58–63.

[25] C. Gabriel, S. Gabriel, and E. Corthout, "The dielectric properties of biological tissues: I. Literature survey," *Physics in Medicine and Biology*, vol. 41, no. 11, pp. 2231–2249, 1996.

[26] S. Gabriel, R. W. Lau, and C. Gabriel, "The dielectric properties of biological tissues: II. Measurements in the frequency range 10 Hz to 20 GHz," *Physics in Medicine and Biology*, vol. 41, no. 11, pp. 2251–2269, 1996.

[27] ——, "The dielectric properties of biological tissues: III. Parametric models for the dielectric spectrum of tissues," *Physics in Medicine and Biology*, vol. 41, no. 11, pp. 2271–2293, 1996.

[28] M. Ulbrich, B. Marleaux, J. Mühlsteff, F. Schoth, R. Koos, D. Teichmann, and S. Leonhardt, "High spatial and temporal resolution 4D FEM simulation of the thoracic bioimpedance using MRI scans," *J. Phys.: Conf. Ser.*, vol. 434, no. 1, p. 012074, 2013.

[29] H. Houck and N. W. Gaw, "A new method of accurate frequency measurement," in *Proceedings of The Radio Club of America*, vol. 37, New York City, USA, Dec 1961.

[30] D. Teichmann, A. Kuhn, S. Leonhardt, and M. Walter, "Human motion classification based on a textile integrated and wearable sensor array," *Physiological Measurement*, vol. 34, no. 9, pp. 963–975, 2013.

[31] N. Westerhof, J.-W. Lankhaar, and B. E. Westerhof, "The arterial Windkessel," *Medical & Biological Engineering & Computing*, vol. 47, no. 2, pp. 131–141, 2009.

[32] L. A. Critchley and J. A. Critchley, "A meta-analysis of studies using bias and precision statistics to compare cardiac output measurement techniques," *Journal of clinical monitoring and computing*, vol. 15, no. 2, pp. 85–91, 1999.

[33] E. Alpaydin, *Introduction to Machine Learning*. Cambridge: MIT Press, 2004.